Earthq Eng & Eng Vib (2011) 10: 553-567 **DOI**: 10.1007/s11803-011-0089-6

Rapid repair of severely earthquake-damaged bridge piers with flexural-shear failure mode

Sun Zhiguo[1†], Wang Dongsheng[1‡], Du Xiuli[2‡] and Si Bingjun[3§]

1. *Institute of Road and Bridge Engineering, Dalian Maritime University, Dalian 116026, China*
2. *Key Laboratory of Urban Security and Disaster Engineering of China Ministry of Education, Beijing University of Technology, Beijing 100124, China*
3. *School of Civil Engineering, Dalian University of Technology, Dalian 116024, China*

Abstract: An experimental study was conducted to investigate the feasibility of a proposed rapid repair technique for severely earthquake-damaged bridge piers with flexural-shear failure mode. Six circular pier specimens were first tested to severe damage in flexural-shear mode and repaired using early-strength concrete with high-fluidity and carbon fiber reinforced polymers (CFRP). After about four days, the repaired specimens were tested to failure again. The seismic behavior of the repaired specimens was evaluated and compared to the original specimens. Test results indicate that the proposed repair technique is highly effective. Both shear strength and lateral displacement of the repaired piers increased when compared to the original specimens, and the failure mechanism of the piers shifted from flexural-shear failure to ductile flexural failure. Finally, a simple design model based on the Seible formulation for post-earthquake repair design was compared to the experimental results. It is concluded that the design equation for bridge pier strengthening before an earthquake could be applicable to seismic repairs after an earthquake if the shear strength contribution of the spiral bars in the repaired piers is disregarded and 1.5 times more FRP sheets is provided.

Keywords: bridge piers; rapid repair after earthquakes; flexural-shear failure; carbon fiber reinforced polymers (CFRP); cyclic testing

1 Introduction

Recent events such as the Loma Prieta earthquake in 1989, Northridge earthquake in 1994, Kobe earthquake in 1995, Chi-Chi earthquake in 1999, and the Wenchuan earthquake in 2008, have repeatedly demonstrated the vulnerabilities of RC bridge piers to seismic actions (Li *et al.*, 2008; Brown and Saiidi, 2011). Apart from the victims and the direct economic costs associated with the replacement of these damaged bridge piers, the disruption of crucial roads over a large time period created tremendous difficulties in the logistics of getting assistance to the impacted areas, therefore aggravating the initial consequences of the earthquakes. In the 2008 Wenchuan earthquake, some bridge piers suffered severe damage as shown in Fig. 1 and required either repair or demolition for reconstruction. If damaged bridge piers could be repaired and rehabilitated rapidly, it would be both more economical than demolishing and reconstructing the bridges, and also extremely important for rescue efforts after an earthquake.

To restore the function of the damaged bridges after an earthquake, various repair techniques for earthquake damaged bridge piers with flexural, shear or lap-splice failures have been developed by researchers and practicing engineers. Concrete jacketing (Fukuyama *et al.*, 2000; Lehman *et al.*, 2001), steel jacketing

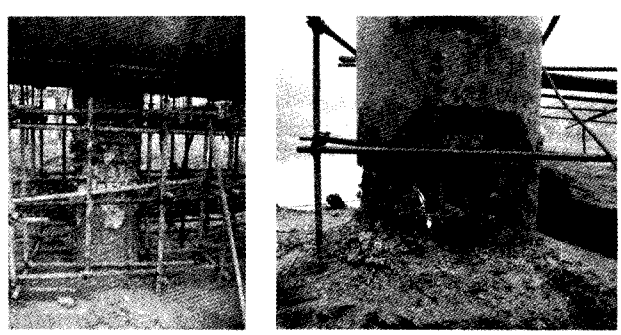

Fig. 1 Representative flexural-shear damage to bridge piers observed after the Wenchuan earthquake

Correspondence to: Wang Dongsheng, Institute of Road and Bridge Engineering, Dalian Maritime University, 1 Linghai Road, Dalian 116026, China
Tel: 86-411-84725098
E-mail: dswang@dlmu.edu.cn
†PhD; ‡Professor; §Associate Professor

Supported by: National Natural Science Foundation of China Under Grant No. 51008041 and 50978042; the National Special Foundation of Earthquake Science of China Under Grant No. 200808021; the Fundamental Research Funds for the Central Universities Under Grant No. 2011JC011
Received June 17, 2011; **Accepted** September 19, 2011

(Aboutaha *et al.*, 1999; Youm *et al.*, 2006) and fiber reinforced polymer (FRP) wrapping (Saadatmanesh *et al.*, 1997; Xiao and Ma, 1997; Li and Sung, 2003; Chang *et al.*, 2004) have been proven to be effective for repairing earthquake damaged bridge piers. Cheng *et al.* (2003, 2005) developed methods to repair earthquake damaged hollow bridge piers, in which new dog-bone shape bars are introduced to replace the fractured longitudinal bars.

Relatively little research, however, has focused on rapid repair techniques for severely earthquake-damaged bridge piers, especially for piers that failed in flexural-shear mode, which was considered to be the main cause of collapse for some bridges during past earthquakes (Hashimoto *et al.*, 2003; Chang *et al.*, 2000; Han *et al.*, 2009; Sun *et al.*, 2008). New techniques are needed that are effective in restoring performance characteristics of these damaged piers and that can be implemented rapidly.

The purpose of the current research is to develop a rapid repair technique for severely earthquake-damaged bridge piers. To fulfill this objective, six original bridge piers with circular sections were designed and tested to severe damage under constant axial load and reversed cyclic displacement excursions. Then the damaged piers were repaired by using early-strength concrete with high-fluidity and carbon fiber reinforced polymer (CFRP) sheets. Finally, a similar test procedure was applied to the repaired bridge piers to check the effectiveness of the repair technique before being used in engineering practice.

2 Experimental program

2.1 Original specimens

Six originally undamaged RC bridge pier specimens representing about 1/3 scale of the prototype piers were designed and constructed, and are designated as specimens A1, A2, A3, A4, A5, and A6, respectively. In designing the longitudinal and spiral reinforcements, the recommendations and requirements specified by the California Department of Transportation (Caltrans, 2001) and the Ministry of Transport of the People's Republic of China (MTPRC, 2008) code for seismic design of the bridge piers with circular sections were considered. The details of the specimens are shown in Fig. 2 and their design parameters are listed in Table 1. All the specimens had a circular section of a diameter of 300 mm and with a heavily reinforced concrete footing. The heights of the piers measured from the footing top surface to the point where the lateral loading was applied are 600 mm for specimens A1, A2, A5 and A6, and 450 and 750 mm for specimens A3 and A4, respectively. Each specimen was fixed at its base to the laboratory strong floor. The specimens contained eight, ten or twelve longitudinal bars of 14 mm in diameter with a measured yielding strength of 327.6 MPa, corresponding to longitudinal reinforcement ratios of 1.74%, 2.18% and 2.61%, respectively. In addition, 6 mm diameter bars with measured yielding strength of 511 MPa were used for spiral bars spaced at 40, 60 or 80 mm, corresponding to volumetric ratios of 1.01%,

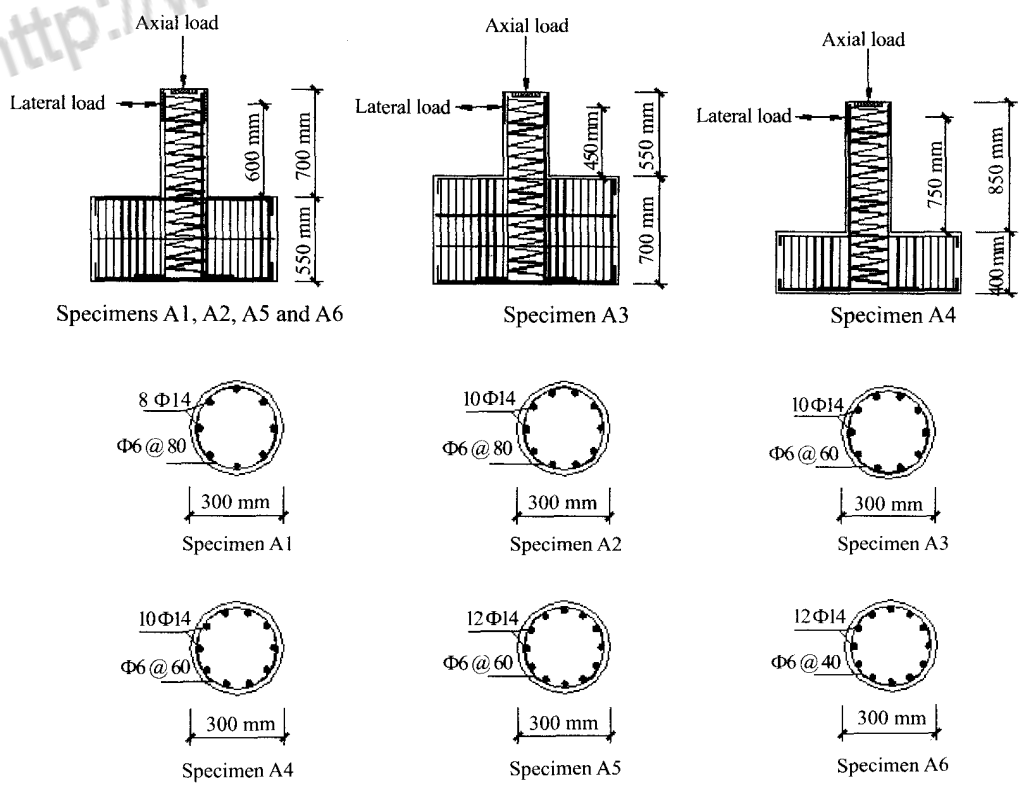

Fig. 2 Details of the original pier specimens

Table 1 Original pier design characteristics details

Specimen	Diameter, D (mm)	Aspect ratio, λ	f_c'(MPa)	Longitudinal bars		Spiral bars		Axial load ratio, $P/A_g f_c'$
				Quantity	ρ_t (%)	s (mm)	ρ_s (%)	
A1	300	2.0	29.4	8Φ14	1.74	80	0.51	0.15
A2	300	2.0	32.2	10Φ14	2.18	80	0.51	0.15
A3	300	1.5	29.4	10Φ14	2.18	60	0.67	0.10
A4	300	2.5	30.1	10Φ14	2.18	60	0.67	0.10
A5	300	2.0	27.3	12Φ14	2.61	60	0.67	0.15
A6	300	2.0	32.2	12Φ14	2.61	40	1.01	0.10

Note: ρ_t is the longitudinal reinforcement ratio; s is spacing of the transverse reinforcement; ρ_s is transverse reinforcement volumetric ratio; P is the axial load of the pier

0.67% and 0.51%, respectively. The actual compression strength of the concrete for each specimen was between 27.3 and 32.2 MPa, as given in Table 1. The specimens had an axial load of 0.10 $A_g f_c'$ or 0.15 $A_g f_c'$, where A_g is the gross cross-sectional area of the pier and f_c' is the concrete compressive strength.

2.2 Testing setup and loading sequence

Both the original and the repaired specimens were tested following the same procedure. The testing setup is shown in Fig. 3.

Strain gauges were installed on the extreme tension and compression sides of the spiral bars and CFRP sheets to measure the strains in the circumferential direction at different loading levels, as shown in Fig. 4. All instrumentations were connected to a data acquisition system and a microcomputer for data recording.

The lateral loading history presented in Fig. 5 was applied to all the original pier specimens. The loading cycles were divided into two phases: load control and displacement control. The former was used to define the pier's experimental yield displacement Δ_y. The displacement controlled loading history included three complete cycles for $u_{\Delta,exp}$=1, 2, 3, ..., until the shear capacity of the pier declined to 85% of the peak load. Here, $u_{\Delta,exp}$ was the ratio of the applied lateral displacement at the top of the pier to the experimental yield displacement Δ_y.

As shown in Fig. 5 (a), the first three cycles of the lateral load were applied to 70% of the theoretical yield load F_y, which was calculated based on moment-curvature analysis using a fiber model (a sectional analysis approach) and measured material properties. The experimental yield displacement Δ_y was determined by extrapolating a straight line from the origin through the measured point corresponding to $0.7F_y$ to the theoretical yield load F_y. The average of the displacement values in both the positive and negative loading directions was used as the experimental yield displacement Δ_y.

As initial lateral stiffness of the repaired pier specimens may be different from that of the companion original specimens, for purposes of comparison, the repaired pier specimens were subjected to the same lateral displacement history as those of the original specimens.

2.3 Damage pattern of the original pier specimens

All the original pier specimens were tested until their lateral load carrying capacity was exhausted, as indicated by a strength reduction exceeding 15% with severe failure. The damage progress of all the original specimens was similar. Horizontal flexural cracks developed first in regions close to the bottom of the specimens. At later stages of loading, they became inclined and extended into the neutral axis

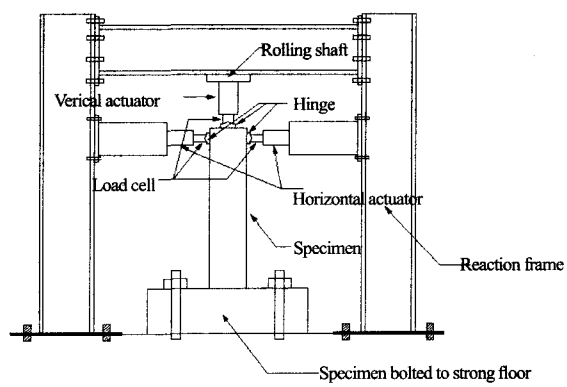

Fig. 3 Testing setup for the original and repaired pier specimens

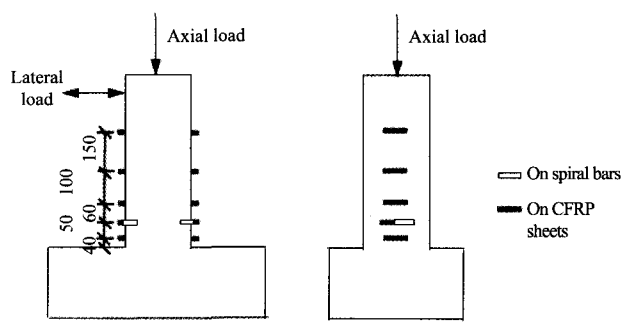

(a) Front view (b) Lateral view

Fig. 4 Location of the strain gauges on spiral bars and the CFRP sheets (Length unit: mm)

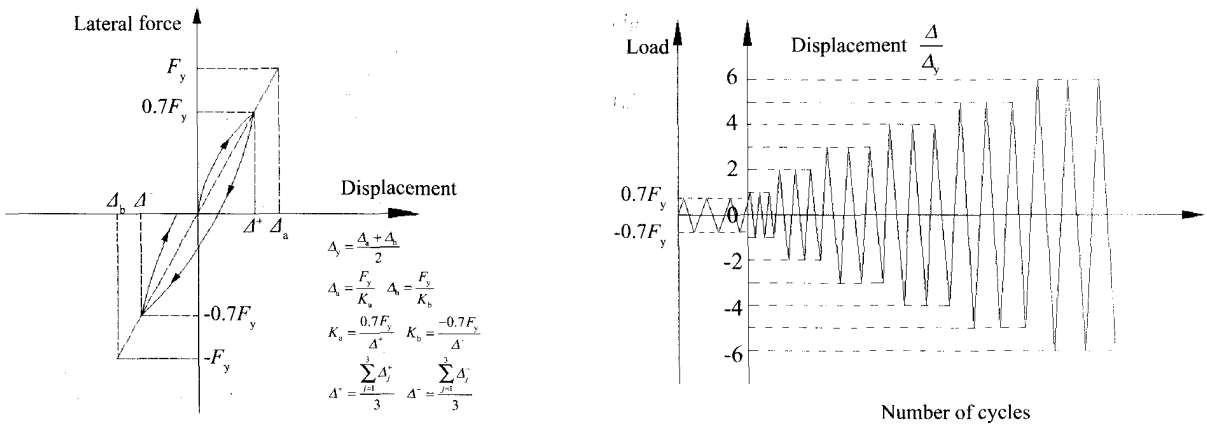

(a) Experimental definition of yield displacement (b) Lateral loading sequence

Fig. 5 Lateral loading sequence for the pier specimens

of the specimens due to the influence of shear. Then, spalling of the concrete cover initiated. Once the cover concrete had completely peeled off and the spiral and longitudinal reinforcement was exposed, longitudinal bar buckling and concrete core crushing followed progressively within next displacement cycles. The ultimate performance of the piers was dominated by shear capacity due to significant diagonal cracking, and in some cases, rupturing of spiral bars. Note that no longitudinal bar rupture was observed in any of the specimens. The damage details of the original pier specimens are summarized in Table 2 and depicted in Fig. 6. The damaged pier specimens were pushed back to their original position (i.e., zero lateral displacement) before the repair operation began.

Table 2 Damage characteristics of the original pier specimens

Specimen	Concrete damage		Reinforcing bar damage	
	Spalled height (mm)	Core crush depth (mm)	No. of buckled longitudinal bars	Spiral bar fractured or not
A1	200	100	5	No
A2	150	Full depth	6	Yes
A3	100	Full depth	6	No
A4	200	Full depth	4	No
A5	210	Full depth	6	Yes
A6	105	100	8	Yes

2.4 Repair procedures and materials

The repair procedures were similar for all the damaged pier specimens and can be summarized as follows: (1) the damaged concrete in and around the damage region was removed, and the pier surface of the damage region was cleaned using a high-pressure air gun; (2) the buckled longitudinal bars were straightened by pounding them with a rubber hammer, and then the fractured spiral bars in specimens A2, A5 and A6 were welded together using new similar reinforcing bars; (3) early-strength concrete with a measured compression strength at 3 days of 31.5 MPa within the damage region was cast, and the surface of the pier specimens was finished to their original shape and dimension. Note that concrete with high fluidity was used in the current study. The proportion for the mixtures of the early-strength concrete with high fluidity is shown in Table 3; (4) a 500 mm wide CFRP sheet was wrapped around the repaired specimen (designated as RA1, RA2, RA3, RA4, RA5 and RA6, respectively) with fiber orientation in the circumferential direction and an overlap length of 150 mm after the early-strength concrete cured for one day. Two layers of CFRP sheets were used for specimens A1, A2, A4 and A6, and three and one layers for specimens A3 and A5, respectively. The CFRP sheet used in this research was 0.167 mm thick, and had a tension strength and modulus of elasticity of 3,995 and 235,000 MPa, respectively. When the CFRP was wrapped around the pier, an epoxy was applied to its surface and the impregnated sheet was tightly wrapped around the pier to ensure that there were no entrapped air pockets or fabric distortions.

Three days after the wrapping, the repaired

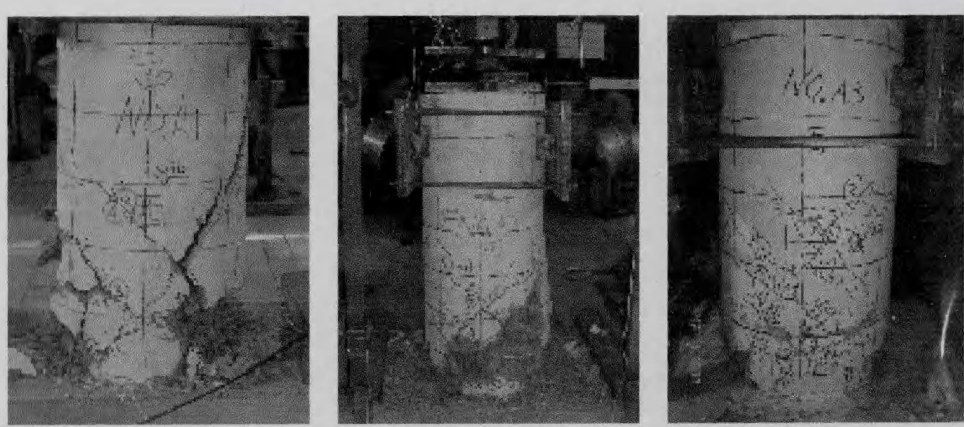

(a) Specimen A1 (b) Specimen A2 (c) Specimen A3

(d) Specimen A4 (e) Specimen A5 (f) Specimen A6

Fig. 6 Final failure patterns of the original pier specimens

Table 3 Mix proportions of early-strength concrete kg/m³

Water	Cement	Fly ash	Sand	Aggregate	Water reducer	Early-strength agent
154	430	120	596	1108	13.75	6.5

specimens were tested to failure again to examine the effectiveness of the repair technique. Note that the overall repair operation of all six specimens lasted about four days.

3 Experimental results of repaired specimens

3.1 Observed behavior

All the repaired specimens behaved in a more ductile behavior than the original specimens. There were no visual signs of damage in any of the specimens during the first three cycles. Then, the first concrete flexural cracks were observed at the pier base where a gap of about 20 mm was intentionally provided to prevent damage to the CFRP sheets. As the lateral displacement increased, the first horizontal cracks appeared on the surface of the CFRP sheets at distances of 125 mm to 230 mm above the base of the specimens and the cracks progressed during the following loading stages. Then, concrete spalling occurred at the base of the pier and the load carrying capacity of the specimen decreased. Fiber ruptured and a snapping noise occurred in specimen RA6 during the last loading cycle. However, neither delamination nor rupture damage of the CFRP sheets was observed in any of the other repaired specimens until the end of the testing. Table 4 summarizes the measured top displacements of the specimens at different damage states. Note that the repair technique delayed the concrete cracking and spalling of the specimens.

The CFRP sheets of the specimens were removed after the test to investigate the damage to the concrete inside. Flexural cracking and slight spalling of the concrete cover were observed within the plastic hinge region of the specimens. However, no significant diagonal shear cracks were found. Thus, it is apparent that the failure mode of the repaired specimens should be identified as flexural failure. Figure 7 shows the failure patterns of the repaired specimens at the end of the testing.

Table 4 Top displacement of the specimens measured at different damage stages

Specimen	Top displacement (mm)		
	First concrete cracking	First CFRP horizontal cracking	Concrete spalling
A1	4.1	—	11.1
RA1	5.4	10.8	37.8
A2	3.1	—	12.8
RA2	4.0	16.0	32.0
A3	1.5	—	9.4
RA3	2.3	6.9	23.0
A4	3.9	—	16.6
RA4	5.5	11.0	38.5
A5	3.8	—	10.7
RA5	5.2	15.6	36.4
A6	5.5	—	11.4
RA6	5.5	10.8	36.4

(a) Specimen RA1 (CFRP removed) (b) Specimen RA2 (c) Specimen RA3 (CFRP removed)

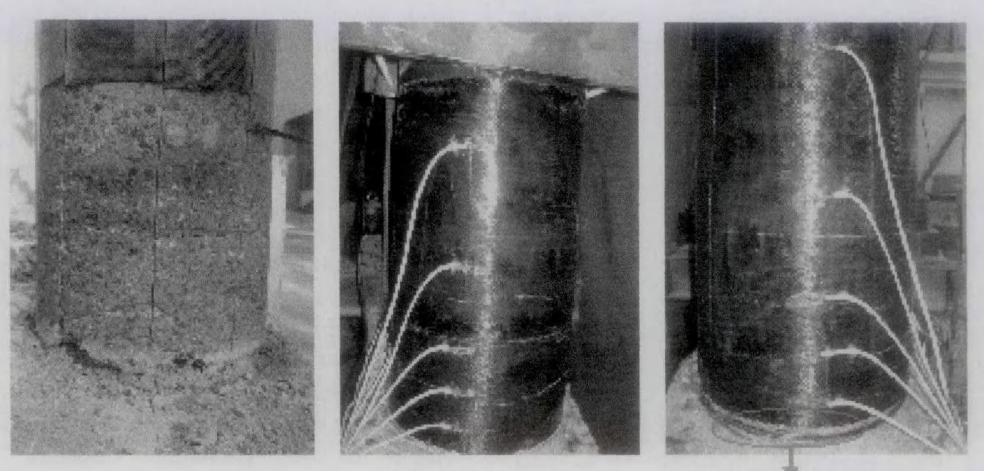

(d) Specimen RA4 (CFRP removed) (e) Specimen RA5 (f) Specimen RA6

Fig.7 Repaired specimens at the end of testing

3.2 Strength, ductility and energy dissipation parameters

The hysteretic curves of the original and repaired pier specimens are plotted in Fig. 8, and their skeleton curves are shown in Fig. 9. In this study, the strength, ductility, and energy dissipation parameters suggested by Sheikh and Khoury (1993), and Légeron and Paultre (2000) are used to evaluate the effectiveness of the proposed repair technique. The associated parameters, including maximum lateral shear strength F_{max}, yield displacement

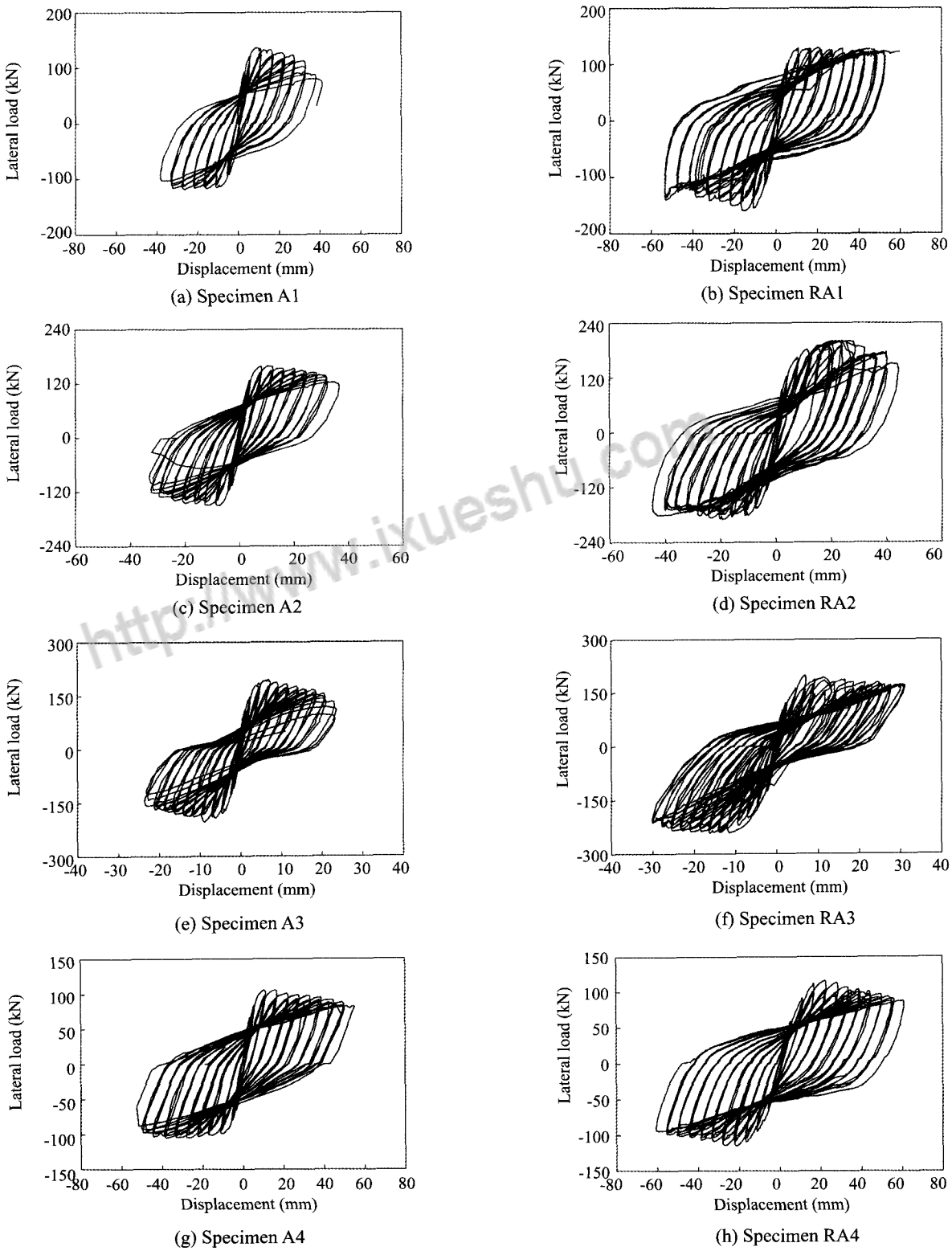

Fig. 8 Hysteretic curves of the original and repaired pier specimens

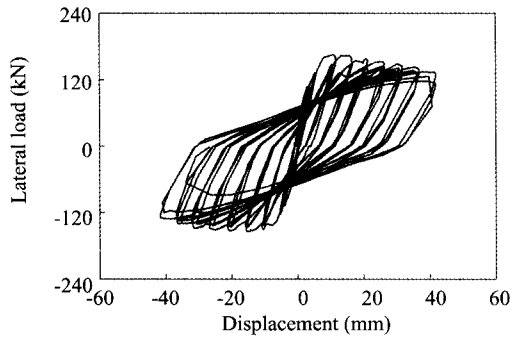

(i) Specimen A5

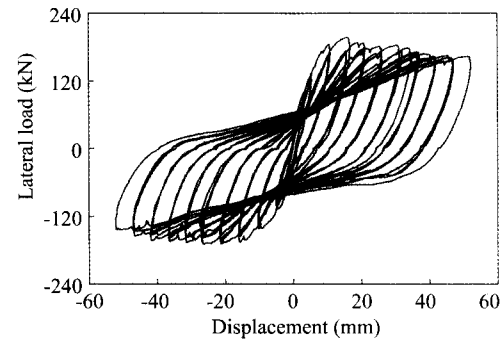

(j) Specimen RA5

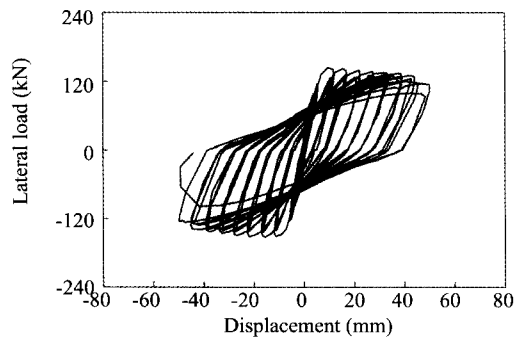

(k) Specimen A6

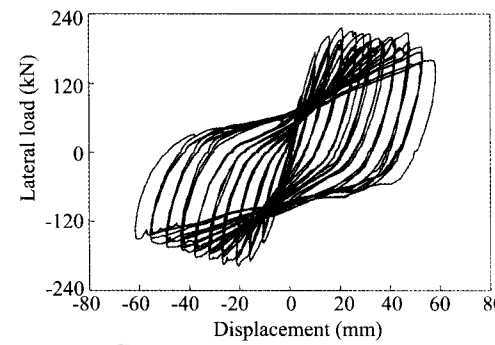

(l) Specimen RA6

Fig. 8 Continued

Δ_1, ultimate displacement Δ_u, displacement ductility factor μ_Δ, ultimate drift ratio R, cumulative displacement ductility ratio N_Δ, and normalized dissipated energy E_N are described in Fig. 10, where m and L represent the number of cycles to failure and the pier height, respectively. Table 5 lists the measured/calculated values of parameters for all tested specimens.

In general, the repaired specimens performed well under the simulated earthquake loading. All the repaired specimens showed a significant improvement in the hysteresis loops and exhibited larger lateral strength and ultimate displacement when compared to the original specimens. Note that all the repaired specimens exhibited much larger yield displacement, which will decrease the displacement ductility factor, cumulative displacement ductility ratio, and the normalized dissipated energy. This is the reason why the ductility and energy dissipation parameters of some of the repaired specimens showed smaller values.

3.3 Lateral stiffness of the piers

For every three cycles at the same lateral displacement Δ, the lateral stiffness K_Δ of the pier is defined as

$$K_\Delta = \frac{K_\Delta^+ + K_\Delta^-}{2} \tag{1}$$

with

$$K_\Delta^+ = \sum_{i=1}^{3} F_{i,\max}^+ / \sum_{i=1}^{3} \Delta_i^+ , \qquad K_\Delta^- = \sum_{i=1}^{3} F_{i,\max}^- / \sum_{i=1}^{3} \Delta_i^- \tag{2}$$

where $F_{i,\max}$ is the maximum lateral load and Δ_i is the corresponding displacement within a cycle at the displacement Δ. The calculated lateral stiffness versus the lateral displacement of the piers before and after repair at each displacement is shown in Fig. 11. Note that the repaired specimens exhibit relatively smaller lateral stiffness during the earlier stage of testing in contrast to the original specimens, which can be explained by pre-existing damage in the tested piers. A close examination of Fig. 11 indicates that the repair technique has influenced the rate of stiffness degradation. All the repaired specimens show a slower rate of stiffness degradation than the original specimens, and the stiffness of the repaired specimens reaches or exceeds that of the original specimens as the lateral displacement increases. This may be because the CFRP sheets delayed the development of damage in the repaired piers.

3.4 Strains in the spiral bars and CFRP sheets

To compare the behavior of the spiral bars in the original and repaired specimens, the strains in the spiral bars at the same location (approximately 90 mm above the top face of the footing) of the original and repaired pier specimens were measured. Figure 12 shows the measured strains in the spiral bars versus the applied lateral displacements. Note that the strains in the spiral bars of the original specimens increased more quickly than those in the repaired specimens. And, the maximum strains reached in the repaired specimens are much

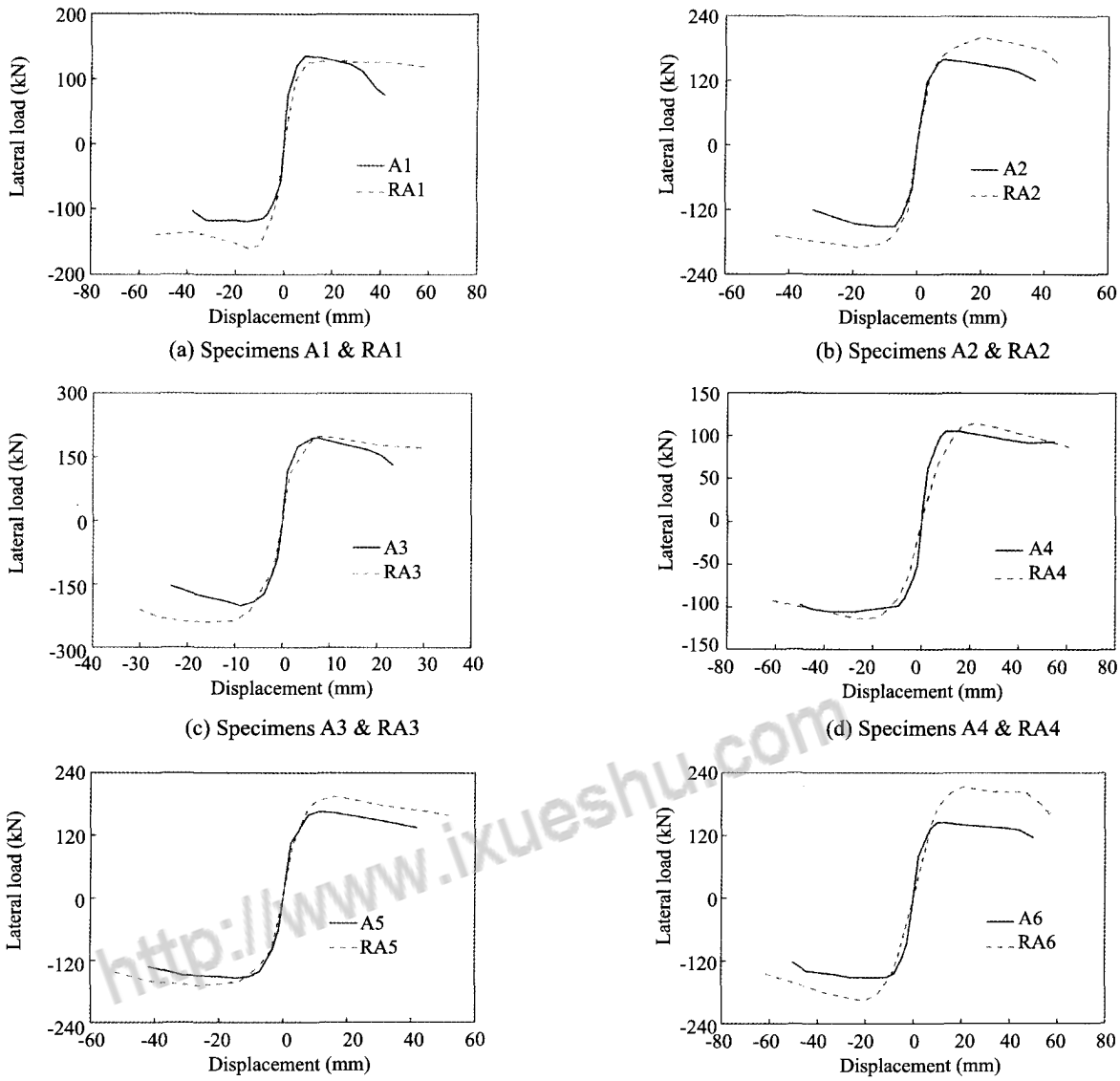

(a) Specimens A1 & RA1 (b) Specimens A2 & RA2

(c) Specimens A3 & RA3 (d) Specimens A4 & RA4

(e) Specimens A5 & RA5 (f) Specimens A6 & RA6

Fig. 9 Skeleton curves for the original and repaired pier specimens

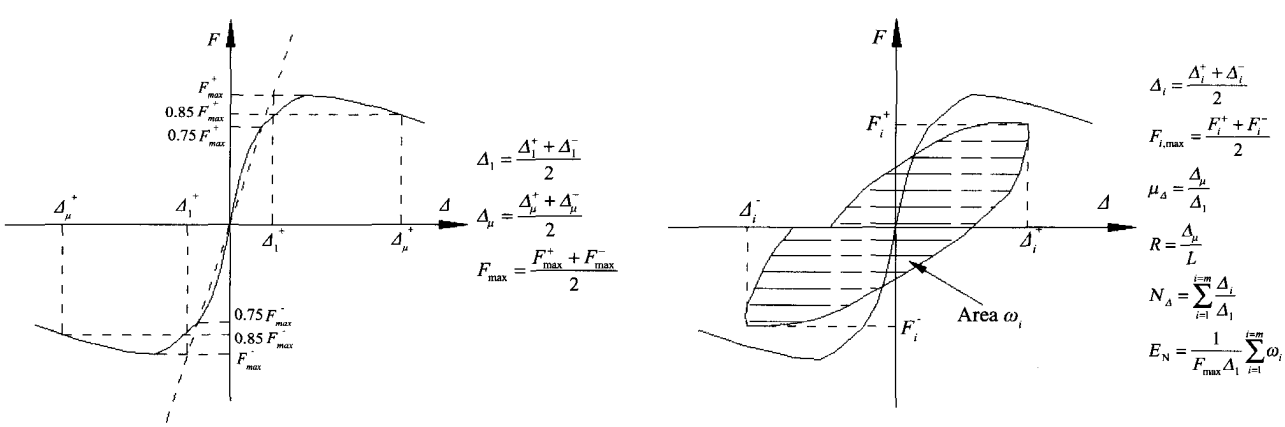

(a) Strength and displacement (b) Ductility and energy dissipation

Fig. 10 Definition of the strength, ductility and energy dissipation parameters

Table 5 Measured / calculated values of strength, ductility and energy dissipation parameters

Specimen	F_{max} (kN)	Δ_1 (mm)	Δ_u (mm)	μ_Δ	R(%)	N_Δ	E_N
A1	127	5.1	34.4	6.75	5.7	48.6	95.0
RA1	144	7.3	47.5	6.51	7.9	104.7	182.6
A2	155	4.5	31.2	6.93	5.2	73.3	125.0
RA2	189	7.1	40.5	5.70	6.8	91.2	127.3
A3	200	3.6	18.5	5.14	4.1	53.1	98.0
RA3	219	6.1	30.0	4.95	6.7	102.0	88.7
A4	105	6.7	48.9	7.30	6.5	86.7	158.1
RA4	115	12.9	52.1	4.04	6.9	42.9	95.5
A5	159	6.1	37.6	6.16	6.3	69.3	110.7
RA5	183	8.8	49.4	5.63	8.2	79.2	107.5
A6	149	6.3	47.1	7.48	7.9	100.2	147.3
RA6	207	12.4	50.3	4.06	8.4	54.7	93.9

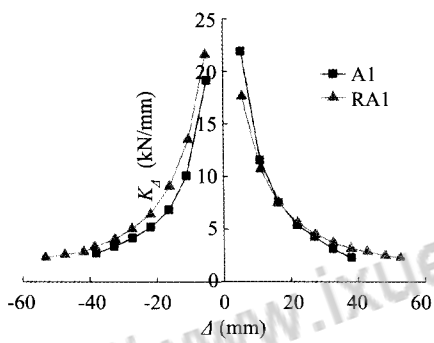

(a) Specimens A1 & RA1

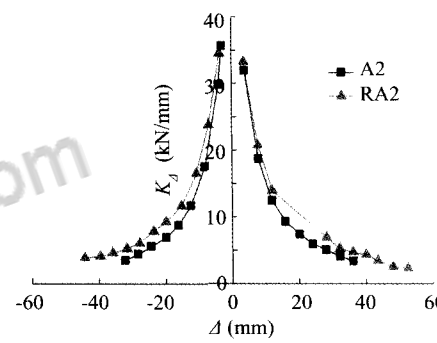

(b) Specimens A2 & RA2

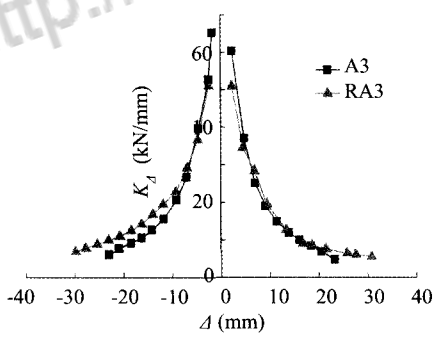

(c) Specimens A3 & RA3

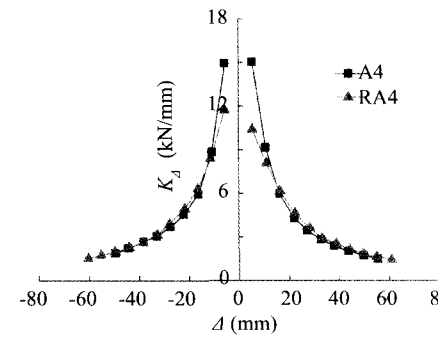

(d) Specimens A4 & RA4

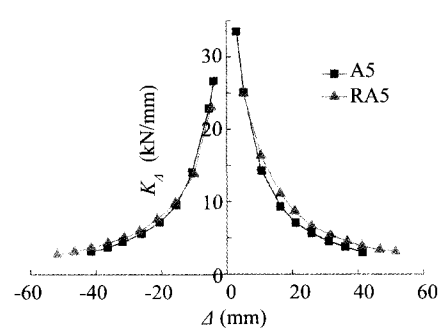

(e) Specimens A5 & RA5

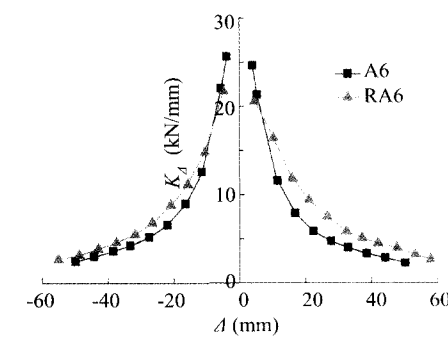

(f) Specimens A6 & RA6

Fig. 11 Comparisons between stiffness-lateral displacement relationships of the original and the company repaired specimens

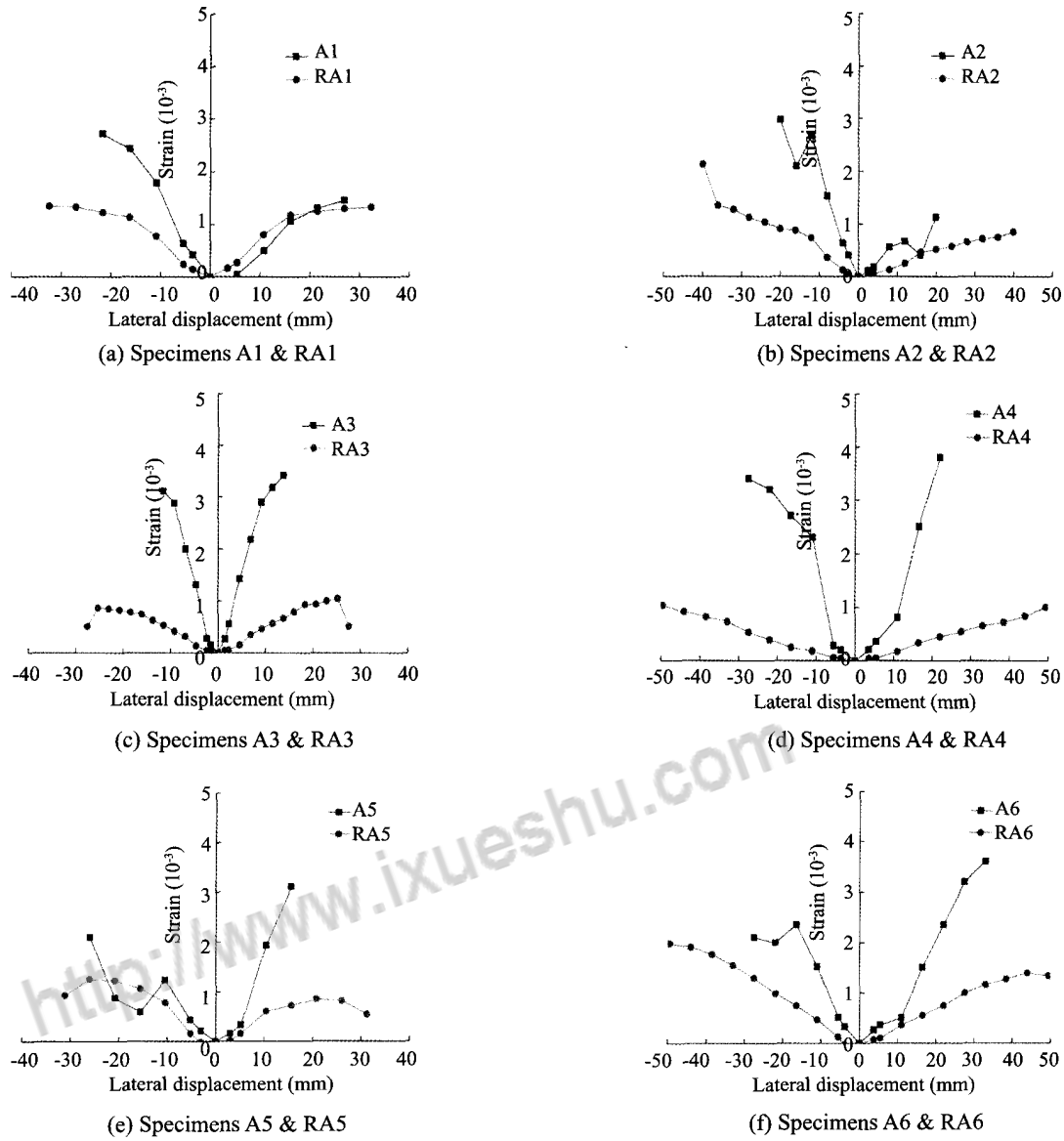

Fig. 12 Comparisons between lateral displacement-strain relationships in the spiral bars of the original and the company repaired specimens

smaller than those in the original specimens at the end of the testing, indicating that the welded spiral bars in the repaired specimens were not as effective as those in the original piers.

The acquisition of strain data on the CFRP sheets is of particular interest to gain a better understanding of the strain profiles of CFRP. Therefore, ten strain gauges were placed on the surface of the CFRP sheets at five different levels along the height of the repaired specimens, oriented in the direction of fibers, as shown in Fig. 4. Figure 13 shows the measured distribution of transverse strain in the CFRP. Note that the maximum strains measured in all the repaired specimens are between 0.003 and 0.006, with the exception of specimen RA6, in which the CFRP sheet fractured and the maximum strain was 0.00942 at the end of testing. The measured maximum strains show good agreement with the strain limit of 0.004 suggested by Priestley and Seible (1995) and used in current seismic retrofit design practice (Ozbakkaloglu and Saatcioglu, 2006). Closer examination of the rupture strain of the CFRP in specimen RA6 indicates that the CFRP efficiency factor, defined as the ratio of the actual CFRP hoop rupture strain in CFRP-confined concrete to the CFRP rupture strain from flat coupon test, is 0.554. This agrees well with the average value of 0.586 reported by Lam and Teng (2003) together with Teng and Lam (2004) based on a large experimental database. Of particular interest here is that specimen RA3, the shortest specimen, developed a relatively uniform distribution of CFRP strain along its height, signifying the influence of shear stresses; whereas a linear variation of strain is observed above the plastic hinge region in all the other specimens due to the linear reduction of flexure and associated confinement action.

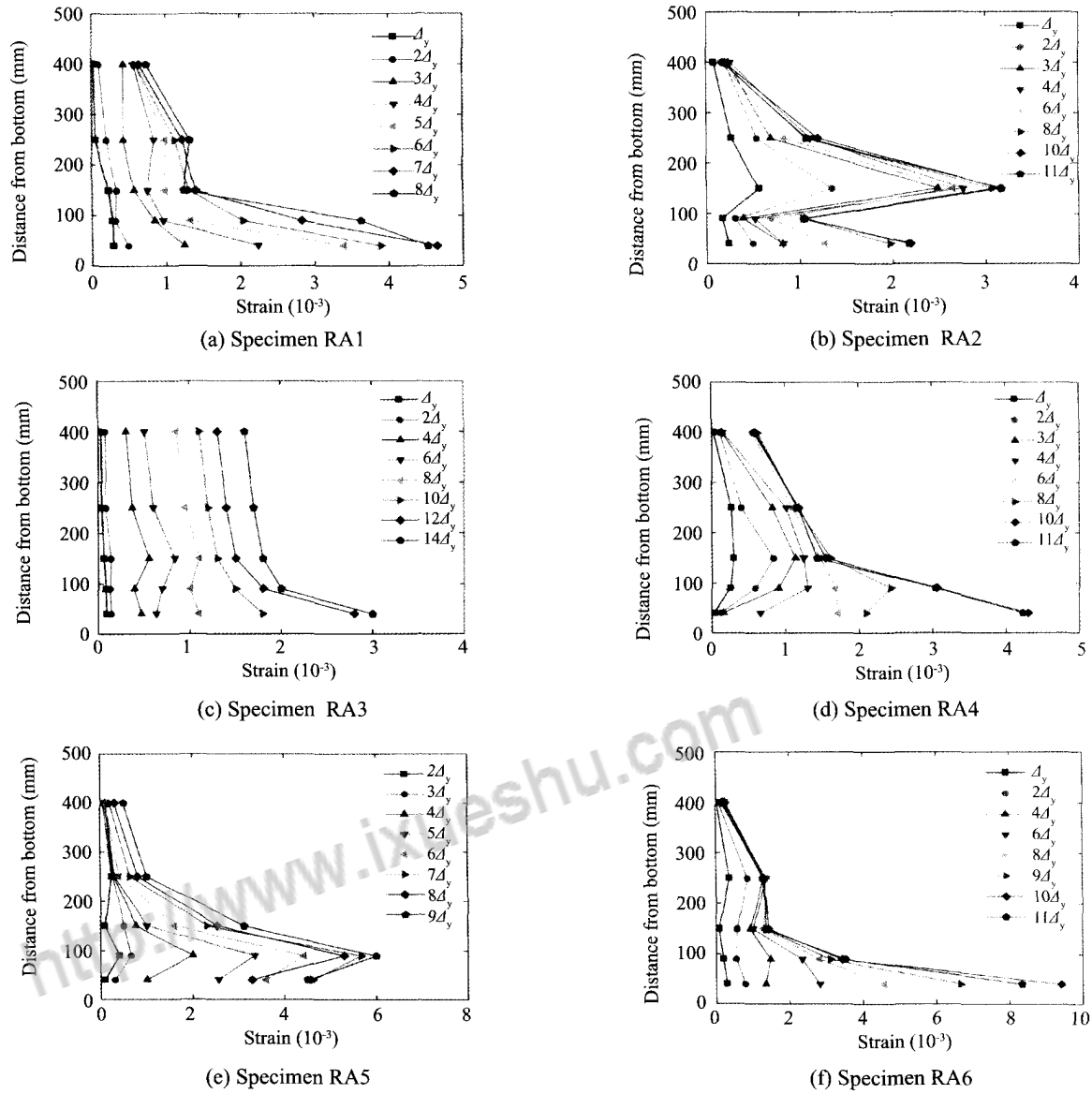

Fig. 13 CFRP strain distribution along the pier height of the repaired specimens

4 Evaluation of design models

Seible *et al.* (1997) recommended that the thickness of the FRP jacket for seismic shear strengthening of circular columns before an earthquake can be determined by

$$t_j = \frac{\frac{V_0}{\phi_v} - V_n}{\frac{\pi}{2} \times 0.004 E_j D} \tag{3}$$

where, t_j is the thickness of the FRP jacket, V_0 is the column shear demand based on full flexural overstrength in the potential plastic hinges, and ϕ_v is the shear capacity reduction factor (typically taken as 0.85). V_n is the shear strength of the bridge piers. E_j and D are FRP modulus and column diameter, respectively.

Various models have been developed to predict the shear strength of bridge piers under seismic action. In the current study, the Priestley model (1994) and the Caltrans model (2001) are used to estimate the shear strength V_n. According to the Priestley model,

$$V_n = V_c + V_s + V_p \tag{4}$$

where

$$V_c = 0.8 A_g k \sqrt{f_c'} \tag{5}$$

$$V_s = \frac{\pi}{2} \frac{A_v f_{yh} D'}{s} \cot 30^\circ \tag{6}$$

and

$$V_p = \frac{P(D-c)}{2a} \tag{7}$$

in which V_c, V_s, and V_p are shear capacity contributions from the concrete, horizontal steel reinforcement, and axial load, respectively. A_v is the cross sectional area of the spiral reinforcement, f_{yh} is the yield strength of the spiral reinforcement, D' is the diameter of the circular hoops, s is the vertical distance between spiral bars, P is the axial load applied to the pier, c is the depth of compression zone, and a is the pier height. The degradation factor k has a value of 0.29 up to a displacement ductility factor μ_Δ of 2.0, and degrades to 0.1 at μ_Δ=4.0, after which it remains constant.

In the Caltrans model, the shear design equation (4) is also valid if the last term V_p is neglected, i.e.,

$$V_n = V_c + V_s \tag{8}$$

where

$$V_c = v_c \times (0.8A_g) \tag{9}$$

$$v_c = \alpha_1 \times \alpha_2 \times \sqrt{f_c'} \le 0.33\sqrt{f_c'} \tag{10}$$

$$0.025 \le \alpha_1 = 0.08\rho_s f_{yh} + 0.305 - 0.083\mu_\Delta < 0.25 \tag{11}$$

$$\alpha_2 = 1 + \frac{P}{13.8A_g} < 1.5 \tag{12}$$

$$V_s = \frac{\pi}{2}\frac{A_v f_{yh} D'}{s} \tag{13}$$

ρ_s is the ratio of the transverse reinforcement volume to column core volume.

To examine the applicability of Eq. (3) to seismic repairs after an earthquake, the analytical modeling is compared to the experimental results. As the experimental results mentioned above reveal that the spiral bars in the repaired pier specimens are not as effective as the original specimens, the shear strength contribution V_s is disregarded in this study. Also, as the shear strength of the concrete component is reduced as the lateral displacement increases, in evaluating V_c using the Priestley and Caltrans model the displacement ductility factor is taken as 4.0 for specimens that failed in flexural-shear mode in this study.

The predicted CFRP thicknesses from Eq. (3) are compared to the experimental data, as shown in Table 6. For the Priestley model, note that the repaired pier specimens were wrapped with 1.57 to 2.46 times as much CFRP sheets as specified by Eq. (3), with an exception of specimen RA5, which was wrapped with only 70 percent of the required CFRP sheet. For the Caltrans model, the repaired specimens were wrapped with 1.35 to 4.03 times as much CFRP sheets as Eq. (3), with an exception of specimen RA5, which was wrapped with only 76 percent of the required CFRP sheet. Note that all the repaired specimens performed well even though the strength and ductility behavior of the repaired piers were not proportional to the amount of CFRP sheets. For the Priestley and Caltrans models, the repaired specimens were wrapped with an average of 1.7 and 1.9 times more CFRP sheets, respectively. Before further study is performed, it is suggested that the design equation proposed by Seible for seismic strengthening of bridge piers before an earthquake be used in seismic repairs after an earthquake if 1.5 times more FRP sheets are provided to insure the effectiveness of the repair.

Table 6 Comparison of experimental and theoretical CFRP thickness and repair effectiveness

Specimen	Thickness of CFRP of the repaired specimens					Repair effectiveness	
	Provided $t_{j\text{-}exp}$ (mm)	Required (mm)		Provided/ Required		$V_{max,rep}/V_{max,ori}$	$\Delta_{u,rep}/\Delta_{u,ori}$
		$t_{j\text{-}Pri}$	$t_{j\text{-}Cal}$	$t_{j\text{-}exp}/t_{j\text{-}Pri}$	$t_{j\text{-}exp}/t_{j\text{-}Cal}$		
A1 & RA1	0.334	0.166	0.201	2.02	1.66	1.13	1.38
A2 & RA2	0.334	0.207	0.247	1.61	1.35	1.22	1.30
A3 & RA3	0.501	0.273	0.253	1.84	1.98	1.10	1.62
A4 & RA4	0.334	0.136	0.083	2.46	4.03	1.10	1.07
A5 & RA5	0.167	0.239	0.219	0.70	0.76	1.15	1.31
A6 & RA6	0.334	0.213	0.185	1.57	1.80	1.39	1.07

5 Conclusions

In this paper, an experimental study to evaluate the effectiveness of the proposed rapid repair technique for earthquake-damaged bridge piers with flexural-shear failure mode was described. First, six circular pier specimens were tested to severe damage under constant axial load and reversed cyclic displacement excursions. Then the damaged specimens were rapidly repaired using early-strength concrete and CFRP sheets and tested to failure again. The seismic performance of the repaired specimens was evaluated and compared to the original specimens. Finally, a simple analytical model for post-earthquake repair design was evaluated and compared with the experimental results. Based on the results of the experimental program, the following

conclusions are reached:

(1) The proposed repair technique is rapid and highly effective. The damaged piers could be repaired within four days, and exhibited both higher strength and lateral displacement than the original piers. And, the failure mechanism of the piers shifted from flexural-shear failure to ductile flexural failure.

(2) The repaired specimens exhibited relatively smaller lateral stiffness during the earlier stages of testing compared to the original specimens as a result of the pre-existing damage. However, during subsequent stages, the lateral stiffness degraded slowly and reached or exceeded that of the original specimens as the lateral displacement increased.

(3) The welded spiral bars in the repaired specimens were not effective compared to those in the original specimens. The strains measured on the surface of the CFRP sheets correspond well with the strain limit of 0.004 often used in current seismic retrofit design practice for bridge columns before an earthquake.

(4) The design equation of Seible *et al.* (1997) for bridge pier strengthening before an earthquake is also applicable for seismic repair after an earthquake with the following conditions: the shear strength of the bridge piers is estimated by using the Priestley model (1994) or the Caltrans model (2001) if the shear strength contribution of the spiral bars in the repaired specimens is disregarded and 1.5 times more FRP sheets are provided. However, note that only a limited number of specimens were tested and to validate this conclusion, further studies are needed.

Acknowledgement

The authors gratefully acknowledge the support of the National Natural Science Foundation of China under Grant No. 51008041 and No. 50978042, the National Special Foundation of Earthquake Science of China under Grant No. 200808021, and the Fundamental Research Funds for the Central Universities under Grant No. 2011JC011.

References

Aboutaha RS, Engelhardt MD, Jirsa JO and Kreger ME (1999), "Experimental Investigation of Seismic Repair of Lap Splice Failures in Damaged Concrete Columns," *ACI Structural Journal*, **96**(2): 297–306.

Brown A and Saiidi MS (2011), "Investigation of Effect of Near-fault Motions on Substandard Bridge Structures," *Earthquake Engineering and Engineering Vibration*, **10**(1): 1–11.

Caltrans (2001), *Seismic Design Criteria*, California Department of Transportation, Sacramento, California.

Chang KC, Chang DW, Tsai MH and Sung YC (2000), "Seismic Performance of Highway Bridges," *Earthquake Engineering and Engineering Seismology*, **2**(1): 55–80.

Chang SY, Li YF and Loh CH (2004), "Experimental Study of Seismic Behavior of As-Built and Carbon Fiber Reinforced Plastics Repaired Reinforced Concrete Bridge Columns," *Journal of Bridge Engineering*, ASCE, **9**(4): 391–402.

Cheng CT, Mo YL and Yeh YK (2005), "Evaluation of As-built, Retrofitted, and Repaired Shear-critical Hollow Bridge Columns under Earthquake-type Loading," *Journal of Bridge Engineering*, ASCE, **10**(5): 520–529.

Cheng CT, Yang JC, Yeh YY and Chen SE (2003), "Seismic Performance of Repaired Hollow-bridge Piers," *Construction and Building Materials*, **17**(5): 339–351.

Fukuyama K, Higashibata Y and Miyauchi Y (2000), "Studies on Repair and Strengthening Methods of Damaged Reinforced Concrete Columns," *Cement & Concrete Composites*, **22**(1): 81–88.

Han Q, Du XL, Liu JB, Li ZX, Li LY and Zhao JF (2009), "Seismic Damage of Highway Bridges During the 2008 Wenchuan Earthquake," *Earthquake Engineering and Engineering Vibration*, **8**(2): 263–273.

Hashimoto S, Fujino Y and Abe M (2003), "Damage Analysis of Hanshin Expressway Viaducts During 1995 Kobe Earthquake. II: Damage Mode of Single Reinforced Concrete Piers," *Journal of Bridge Engineering*, ASCE, **10**(1): 54–60.

Lam L and Teng JG (2003), "Design-oriented Stress-strain Model for FRP-confined Concrete," *Construction and Building Materials*, **17**(6-7): 471–489.

Légeron F and Paultre P (2000), "Behavior of High-strength Concrete Columns under Cyclic Flexure and Constant Axial Load," *ACI Structural Journal*, **97**(4): 591–601.

Lehman DE, Gookin SE, Nacamuli MN and Moehle JP (2001), "Repair of Earthquake-damaged Bridge Columns," *ACI Structural Journal*, **98**(2): 233–245.

Li J Z, Peng T B and Xu Y(2008), "Damage Investigation of Girder Bridges under the Wenchuan Earthquake and Corresponding Seismic Design Recommendations," *Earthquake Engineering and Engineering Vibration*, **7**(4): 337–344.

Li YF and Sung YY (2003), "Seismic Repair and Rehabilitation of a Shear-faliure Damaged Circular Bridge Column Using Carbon Fiber Reinforced Plastic Jacketing," *Canadian Journal of Civil Engineering*, **30**(5): 819–829.

Ministry of Transport of the People's Republic of China (MTPRC) (2008), *Guidelines for Seismic Design of Highway Bridges* (*JTG/T B02-01 2008*), Beijing. (in Chinese).

Ozbakkaloglu T and Saatcioglu M (2006), "Seismic Behavior of High-strength Concrete Columns Confined by Fiber-reinforced Polymer Tubes," *Journal of Composites for Construction*, ASCE, **10**(6): 538–549.

Priestley MJN and Seible F (1995), "Design of Seismic Retrofit Measures for Concrete and Masonry Structures," *Construction and Building Materials*, **9**(6): 365–377.

Priestley MJN, Verma R and Xiao Y (1994), "Seismic Shear Strength of Reinforced Concrete Columns," *Journal of Structural Engineering*, ASCE, **120**(8): 2310–2329.

Saadatmanesh H, Ehsani MR and Jin LM (1997), "Repair of Earthquake-damaged RC Columns with FRP Wraps," *ACI Structural Journal*, **94**(2): 206–215.

Seible F, Priestley MJN, Hegemier GA and Innamorato D (1997), "Seismic Retrofit of RC Columns with Continuous Carbon Fiber Jackets," *Journal of Composites for Construction*, ASCE, **1**(2): 52–62.

Sheikh SA and Khoury SS (1993), "Confined Concrete Columns with Stubs," *ACI Structural Journal*, **90**(4): 414–431.

Sun ZG, Si BJ, Wang DS and Guo X (2008), "Experimental Research and Finite Element Analysis of Bridge Piers Failed in Flexure-shear Modes," *Earthquake Engineering and Engineering Vibration*, **7**(4): 403–414.

Teng JG and Lam L (2004), "Behavior and Modeling of Fiber Reinforced Polymer-confined Concrete," *Journal of Structural Engineering*, ASCE, **130**(11): 1713–1723.

Xiao Y and Ma R (1997), "Seismic Retrofit of RC Circular Columns Using Prefabricated Composite Jacketing," *Journal of Structural Engineering*, ASCE, **123**(10): 1357–1364.

Youm KS, Lee HE and Choi S (2006), "Seismic Performance of Repaired RC Columns," *Magazine of Concrete Research*, **58**(5): 267–276.